Available online at www.sciencedirect.com

ScienceDirect

Advances in Space Research 66 (2020) 2516–2527

ADVANCES IN SPACE RESEARCH (a COSPAR publication)

www.elsevier.com/locate/asr

Evaluating the impact of CNES real-time ionospheric products on multi-GNSS single-frequency positioning using the IGS real-time service

Ahao Wang [a,b], Junping Chen [b,c,d,*], Yize Zhang [b,e], Lingdong Meng [a,b], Binghao Wang [f], Jiexian Wang [a]

[a] College of Surveying and Geo-Informatics, Tongji University, Shanghai 200092, China
[b] Shanghai Astronomical Observatory, Chinese Academy of Sciences, Shanghai 200030, China
[c] School of Astronomy and Space Science, University of Chinese Academy of Sciences, Beijing 100049, China
[d] Shanghai Key Laboratory of Space Navigation and Positioning Techniques, Shanghai Astronomical Observatory, Chinese Academy of Sciences, Shanghai 200030, China
[e] Tokyo University of Marine Science and Technology, Tokyo 1358533, Japan
[f] Beijing Navigation Center, Beijing 100094, China

Received 9 May 2020; received in revised form 27 August 2020; accepted 3 September 2020
Available online 19 September 2020

Abstract

Multi-global navigation satellite system (GNSS) real-time (RT) single-frequency (SF) positioning with a low-cost receiver has received increasing attention in recent years due to its large amount of possible applications. One major challenge in single-frequency positioning is the effective mitigation of the ionospheric delays since it is a dominant error source. Nowadays, a high-precision RT ionospheric vertical total electron content (VTEC) product is released by the Centre National d'Etudes Spatiales (CNES) through its real-time service (RTS). The effect of this product on RT single-frequency positioning needs to be investigated. In this study, we provide an evaluation of the quality of multi-GNSS CLK93 orbit and clock products through the comparison to the final precise products, and comprehensively evaluate the impact of CNES VTEC products on multi-GNSS RT-SF-SPP (Standard Point Positioning)/PPP (Precise Point Positioning) performances. Datasets from 46 Multi-GNSS Experiment (MGEX) stations and the CLK93 corrections for 14 consecutive days in 2019 are collected to process with different scenarios. Experimental results show that the CNES VTEC products can replace the final GIM products in the single- and multi-GNSS SF-SPP with the same positioning accuracy requirements during the period of mild solar activity (Kp index is less than 3). Regarding the kinematic RT-SF-PPP, the (re-)convergence also can be improved by adopting the prior CNES-VTEC constrains. Compared with the IF RT-SF-PPP with quad-constellation, the positioning accuracy of the CNES-VTEC-constrained RT-SF-PPP can be improved by about 10.30%, in which the average RMS can achieve 17.9, 19.8 and 32.3 cm in the North, East and Up components, respectively.

Compared with the final precise products of GBM, the satellite orbit accuracy of CLK93 products is 4, 5, 12 and 16 cm for GPS, Galileo, GLONASS and BDS, respectively. As for the CLK93 satellite clock, its RMS accuracy of GPS, Galileo, GLONASS and BDS is 0.3, 0.4, 2.5 and 1.8 ns, respectively.

Keywords: Multi-GNSS; Real-time; Single frequency; SPP; PPP; CNES-VTEC

* Corresponding author at: Shanghai Astronomical Observatory, Chinese Academy of Sciences, Shanghai 200030, China.
E-mail addresses: ahao_wang@tongji.edu.cn (A. Wang), junping@shao.ac.cn (J. Chen), 13zhyize@tongji.edu.cn (Y. Zhang), ldmeng@tongji.edu.cn (L. Meng), wangjiexian@tongji.edu.cn (J. Wang).

https://doi.org/10.1016/j.asr.2020.09.010
0273-1177/

1. Introduction

With the rapid development of multi-frequency and multi-global navigation satellite system (GNSS), standard point positioning (SPP) and precise point positioning (PPP), as the absolute positioning techniques with a stand-alone GNSS receiver, has been widely used in numerous fields such as vehicle navigation, meteorology and natural hazard monitoring(Zumberge et al., 1997; Kouba and Heroux, 2001; Zhang and Andersen, 2006; Jin et al., 2017; Wang et al., 2019b). In general, dual-frequency (DF) PPP has the ability to provide millimeter-level and centimeter-level positioning accuracy in static and kinematic mode, respectively (Li et al., 2011, 2013). However, the cost of the geodetic multi-frequency GNSS receiver limits its commercial application, and a great number of possible real-time applications only require sub-meter-level or decimeter-level positioning accuracy. Therefore, real-time single-frequency precise point positioning (RT-SF-PPP) with a low-cost receiver has attracted great attention in the GNSS market (van Bree and Tiberius, 2012; de Bakker and Tiberius, 2017; Odolinski and Teunissen, 2017).

The biggest error source for single-frequency positioning is the ionospheric delay, as it cannot be eliminated precisely and may lead to the range errors of 100 m in navigation signal during solar activity (Liu and Yang, 2016). Nowadays, several broadcast ionospheric models can be employed to mitigate the ionospheric effect in RT single-frequency positioning. The Klobuchar model broadcasted in the broadcast ephemeris is widely used by both GPS and GLONASS users in RT mode, which has the advantages of simple structure and high efficiency, but the ionospheric errors can only be mitigated by 50% (Feess and Stephens, 1987; Klobuchar, 1987). For the European Galileo, a high complexity model named NeQuick has been established and can mitigate approximately 70% ionospheric errors for single-frequency users (Bidaine, 2012). As to the second phase of the Chinese BeiDou navigation satellite system (BDS-2), the satellites broadcast an improved Klobuchar model named CIM (COMPASS Ionospheric Model), which can correct for around 65% of the ionospheric errors (Wu et al., 2013). With the completion of the BDS-3 since the end of 2018, a BeiDou global broadcast ionospheric delay correction model (BDGIM) is proposed and can mitigate around 77% ionospheric errors on the global scale (Yuan et al., 2019). Besides, Hoque and Jakowski (2015) proposed an alternative ionospheric correction algorithm called Neustrelitz TEC broadcast model (NTCM-BC), its performance is comparable to the NeQuick model and as easy to compute as the Klobuchar model. Although these above-mentioned ionospheric models support RT processing, their relatively low accuracy of the ionospheric model cannot meet the requirements of high-precision RT single-frequency users.

Since 1 April 2013, an open-access real-time service (RTS) has been launched by the International GNSS Service (IGS). Currently, available RTS products, including the satellite orbit corrections, clock corrections, code bias and phase bias as well as the vertical total electron content (VTEC) message, are formatted into state space representation (SSR) messages (RTCM Special Committee 2016). Using these messages, RT-PPP can be conducted by GNSS single or multi-frequency receivers anywhere in the world. the Centre National d'Etudes Spatiales (CNES) is providing the VTEC products and other corrections though its two RTS streams (CLK92 and CLK93) including GPS, GLONASS, BDS and Galileo satellites (Zhang et al., 2019a). Roma et al. (2016) showed the initial results of CNES VTEC products referenced to six different Global Ionospheric Maps (GIMs) for 15 days. Nie et al. (2019) evaluated the quality of CNES VTEC products for 374 consecutive days and conducted RT-SF-PPP experiments using Multi-GNSS Experiment (MGEX) static data and automotive kinematic data. The result showed that the root mean square (RMS) of CNES VTEC products compared with the IGS final GIM is about 1–3 TECU, and the RT-SF-PPP using this ionosphere product can achieve sub-meter-level and meter-level positioning accuracy in horizontal and vertical components, respectively. To improve the convergence of RT-PPP, the CNES VTEC products are applied to undifferenced and uncombined RT-PPP as an extra constraint due to their high-precision (Liu et al., 2018). On the one hand, the majority of current contributions mainly focused on the validation and performance evaluation of RT-DF-PPP using RTS orbit and clock corrections. On the other hand, the previous studies only concerned the contribution of CNES VTEC products to single- or dual-constellation (e.g. GPS/GLONASS, GPS/Galileo) SF-PPP users. With the development of multi-GNSS and IGS RTS, it is necessary to perform more comprehensively performance evaluation of RT-SF-PPP with quad-constellation using the CNES VTEC products as a priori constrain. Besides, up to now, there is no literature dedicated to the impact of CNES VTEC products on SF-SPP positioning performance. The numerical results will be generated in this work.

Firstly, we briefly introduce the GPS + GLONASS + BDS + Galileo combined model for SF-SPP/PPP and RT processing strategies. Next, the quality of RT orbit, clock and VTEC messages from the CLK93 stream is investigated. Thereafter, a comprehensive analysis of the contribution of CNES VTEC products to multi-GNSS SF-SPP/PPP is performed. Finally, some findings of this paper are summarized.

2. Multi-GNSS positioning models

The original multi-GNSS code and phase observation equations on the frequency i at a particular epoch can be expressed as (Li et al., 2015)

$$\begin{cases} P_{r,i}^{s,Q} = \rho_r^{s,Q} + c(dt_r - dt^{s,Q}) + \theta^{s,Q} + Trop_r^{s,Q} + Iono_{r,i}^{s,Q} \\ \qquad + d_{r,i} - d_i^{s,Q} + \omega_{r,i}^{s,R} + \varepsilon_{r,i}^{s,Q} \\ \Phi_{r,i}^{s,Q} = \rho_r^{s,Q} + c(dt_r - dt^{s,Q}) + \theta^{s,Q} + Trop_r^{s,Q} - Iono_{r,i}^{s,Q} \\ \qquad + \lambda_i^{s,Q} \cdot N_{r,i}^{s,Q} + b_{r,i} - b_i^{s,Q} + \xi_{r,i}^{s,Q} \end{cases} \tag{1}$$

where the indices s, r and i represent the satellite, receiver and frequency, respectively. The superscript Q is satellite system (i.e. G for GPS, R for GLONASS, C for BDS, E for Galileo). $P_{r,i}^{s,Q}$ and $\Phi_{r,i}^{s,Q}$denote the observed code and phase in meters, respectively; $\rho_r^{s,Q}$ is the geometric range between the satellite and receiver antennas in meters; $c$is the light velocity in meters per second; $dt_r$and $dt^{s,Q}$are the receiver and satellite clock offsets in seconds, respectively. $\theta^{s,Q}$ is the satellite orbit error in meters; $Trop_r^{s,Q}$ and $Iono_{r,i}^{s,Q}$ is the slant tropospheric delay and slant ionospheric delay in meters, respectively; $\lambda_i^{r,Q}$ is the carrier wavelength of frequency i in meters per cycle; $N_{r,i}^{s,Q}$ is the integer phase ambiguity in cycles; $d_{r,i}$ and $d_i^{s,Q}$ are code hardware delays for the receiver and satellite in meters, respectively; $b_{r,i}$ and $b_i^{s,Q}$ are phase hardware delays for the receiver and satellite in meters, respectively. Different from other satellite systems, GLONASS adopts frequency division multiple access (FDMA) technique to distinguish signals from different satellites, the GLONASS satellite-specific frequency-dependent biases (i.e., inter-frequency biases, IFBs) $\omega_{r,i}^{s,R}$ need to be considered. In our study, the IFBs are modeled as a linear function of channel numbers in SF-PPP. $\varepsilon_{r,i}^{s,Q}$and $\xi_{r,i}^{s,Q}$ are the noise of code and phase measurements in meters.

2.1. Single-frequency SPP

SPP plays a vital role in the RT positioning, navigation and timing (PNT) services due to its simple model and high calculating efficiency. As for SF-SPP, the three-dimensional (3D) coordinates of receiver x and receiver clock error dt_r can be determined by at least four satellites observations. The satellite orbit $\theta^{s,Q}$ and clock $dt^{s,Q}$ are calculated from the broadcast ephemeris. Both tropospheric errors $Trop_r^{s,Q}$ and ionospheric errors $Iono_{r,i}^{s,Q}$ are usually corrected by the external models. Besides, noted that the inter-system bias (ISB) parameters should be estimated in multi-GNSS processing since the different constellations have different time systems (Wanninger, 2012; Torre and Caporali, 2015; Zhou et al., 2019). The GPS receiver clock is selected generally as a reference, hence, the GPS + GLONASS + BDS + Galileo SF-SPP models can be rewritten as

$$\begin{cases} P_{r,i}^{s,G} = x_r + c \cdot d\bar{t}_r + \varepsilon_{r,i}^{s,G} \\ P_{r,i}^{s,R/C/E} = x_r + c \cdot (d\bar{t}_r + ISB_r^{R/C/E}) + \varepsilon_{r,i}^{s,R/C/E} \end{cases} \tag{2}$$

$$d\bar{t}_r = dt_r + d_{r,i} \tag{3}$$

where $d\bar{t}_r$ is the new GPS receiver clock offset containing the code hardware delay of receiver. The timing group delay (TGD) parameters can be used to correct the satellite code hardware delay. Therefore, three types of parameters to be estimated in multi-GNSS SF-SPP are as follows

$$V = [x, d\bar{t}_r, ISB_r^{R/C/E}] \tag{4}$$

2.2. Ionosphere-free single-frequency PPP

Thanks to the ionospheric delay of one satellite have the same values but with the opposite sign in the code and phase observations, a linear ionospheric-free (IF) combined model named GRoup And PHase Ionospheric Correction (GRAPHIC) is widely utilized in SF-PPP (Cai et al., 2013). Since the number of the GRAPHIC observation equations derived from single-frequency code and phase measurements is half of that of the traditional SF-PPP model, the code observations are required to avoid the rank deficiency (Montenbruck, 2003). It is worth noting that the ionospheric delay in the code observations is corrected by the CNES VTEC products from the CLK93 stream in this study. As to the tropospheric delay, most of them are corrected by the external model, and the residual errors are estimated as a random-walk noise process. The CLK93 orbit and clock products are used to fix the satellite orbit and clock offsets in RT-SF-PPP. Thus, the IF multi-GNSS SF-PPP models can be expressed as

$$\begin{cases} P_{r,i}^{s,G} = x + c \cdot d\bar{t}_r + M\mathrm{w}_r^{s,G} \cdot ZWD_r + \varepsilon_{r,i}^{s,G} \\ P_{r,i}^{s,R} = x + c \cdot (d\bar{t}_r + ISB_r^{R}) + M\mathrm{w}_r^{s,R} \cdot ZWD_r + \omega_{r,i}^{s,R} + \varepsilon_{r,i}^{s,R} \\ P_{r,i}^{s,C/E} = x + c \cdot (d\bar{t}_r + ISB_r^{C/E}) + M\mathrm{w}_r^{s,C/E} \cdot ZWD_r + \varepsilon_{r,i}^{s,C/E} \end{cases} \tag{5}$$

$$\begin{cases} \frac{P_{r,i}^{s,G} + \Phi_{r,i}^{s,G}}{2} = x + c \cdot d\bar{t}_r + M\mathrm{w}_r^{s,G} \cdot ZWD_r + \frac{\lambda_i^{s,G} \cdot \bar{N}_{r,i}^{s,G}}{2} + \varepsilon_{r,IF}^{s,G} \\ \frac{P_{r,i}^{s,R} + \Phi_{r,i}^{s,R}}{2} = x + c \cdot (d\bar{t}_r + ISB_r^{R}) + M\mathrm{w}_r^{s,R} \cdot ZWD_r + \frac{\lambda_i^{s,R} \cdot \bar{N}_{r,i}^{s,R}}{2} + \frac{\omega_{r,i}^{s,R}}{2} + \varepsilon_{r,IF}^{s,R} \\ \frac{P_{r,i}^{s,C/E} + \Phi_{r,i}^{s,C/E}}{2} = x + c \cdot (d\bar{t}_r + ISB_r^{C/E}) + M\mathrm{w}_r^{s,C/E} \cdot ZWD_r + \frac{\lambda_i^{s,C/E} \cdot \bar{N}_{r,i}^{s,C/E}}{2} + \varepsilon_{r,IF}^{s,C/E} \end{cases} \tag{6}$$

$$d\bar{t}_r = dt_r + \frac{b_{r,i} + d_{r,i}}{2} \tag{7}$$

where $M\mathrm{w}_r^s$ is the mapping function of zenith tropospheric wet delay; ZWD_r is the zenith tropospheric wet delay in meters; $\varepsilon_{r,IF}^s$ is the noise of IF observations in meters. In summary, six types of parameters to be estimated in IF multi-GNSS SF-PPP are as follows (Li et al., 2020)

$$V = [x, d\bar{t}_r, ZWD_r, ISB_r^{R/C/E}, \omega_{r,i}^{s,R}, \bar{N}_{r,i}^{s,G/R/C/E}] \tag{8}$$

2.3. Ionosphere-constrained single-frequency PPP

In the undifferenced and uncombined SF-PPP, the ionospheric delay can be estimated as an unknown parameter. Many studies have shown that proper constraints for the ionospheric parameter can improve SF-PPP performance, especially in terms of convergence (Choy et al., 2008; Juan et al., 2012; Shi et al., 2012; Zhang et al., 2013). The process strategies of the satellite orbit, satellite clock offsets and the residual tropospheric delay are the same as in Section 2.2. The ionosphere-constrained (IC) SF-PPP can be expressed as

$$\begin{cases} P_{r,i}^{s,G} = x + c\cdot \bar{dt}_r + M\mathrm{w}_r^{s,G}\cdot ZWD_r + Iono_{r,i}^{s,G} + \varepsilon_{r,i}^{s,G} \\ P_{r,i}^{s,R} = x + c(\bar{dt}_r + ISB_r^R) + M\mathrm{w}_r^{s,R}\cdot ZWD_r + Iono_{r,i}^{s,R} + \omega_{r,i}^{s,R} + \varepsilon_{r,i}^{s,R} \\ P_{r,i}^{s,C/E} = x + c(\bar{dt}_r + ISB_r^{C/E}) + M\mathrm{w}_r^{s,C/E}\cdot ZWD_r + Iono_{r,i}^{s,C/E} + \varepsilon_{r,i}^{s,C/E} \end{cases} \quad (9)$$

$$\begin{cases} L_{r,i}^{s,G} = x + c\cdot \bar{dt}_r + M\mathrm{w}_r^{s,G}\cdot ZWD_r - Iono_{r,i}^{s,G} + \lambda_i^{s,G}\cdot \bar{N}_{r,i}^{s,G} + \xi_{r,i}^{s,G} \\ L_{r,i}^{s,R} = x + c(\bar{dt}_r + ISB_r^R) + M\mathrm{w}_r^{s,R}\cdot ZWD_r - Iono_{r,i}^{s,R} + \lambda_i^{s,R}\cdot \bar{N}_{r,i}^{s,R} + \xi_{r,i}^{s,R} \\ L_{r,i}^{s,C/E} = x + c(\bar{dt}_r + ISB_r^{C/E}) + M\mathrm{w}_r^{s,C/E}\cdot ZWD_r - Iono_{r,i}^{s,C/E} + \lambda_i^{s,C/E}\cdot \bar{N}_{r,i}^{s,C/E} + \xi_{r,i}^{s,C/E} \end{cases} \quad (10)$$

$$\gamma = Iono_{r,i}^{s,G/R/C/E} + \varepsilon_\gamma \quad (11)$$

Noted that the above $\bar{dt}_r$ is the same as equation (3). A virtual observation equation (11) is introduced to the SF-PPP to solve the problem of rank deficiency. The setting of the weight of virtual ionospheric constraints can refer to (Zhang et al., 2013; Wang et al., 2019a), and the variance of the zenith ionospheric delay can be defined as 0.25 m^2. Therefore, seven types of parameters to be estimated in IC multi-GNSS SF-PPP are as follows (Li et al., 2020)

$$V = [x, \bar{dt}_r, ZWD_r, ISB_r^{R/C/E}, \omega_{r,i}^{s,R}, Iono_{r,i}^{s,G/R/C/E}, \bar{N}_{r,i}^{s,G/R/C/E}] \quad (12)$$

3. Data description and processing strategy

3.1. Dataset

To evaluate the impact of CNES VTEC products on the multi-GNSS SF-SPP/PPP performance, GPS, GLONASS, BDS and Galileo observation datasets collected from 46 MGEX stations are selected, which covered 14 days of DOY (Day of Year) 117–130 in 2019. These selected stations are globally evenly distributed, as shown in Fig. 1. It should be noted that the datasets are collected in the post mode, whereas SF-SPP/PPP is simulated in the RT mode, where the real-time corrections of orbit, clock and ionospheric data from CLK93 are also archived in files, and later they are read epoch-by-epoch like real-time "stream" and the kinematic solutions are derived.

Fig. 1. Distribution of the selected 46 MGEX stations.

3.2. Processing strategy

A software named Net_Diff was used to conduct SF-SPP/PPP in this test. Net_Diff is a software for GNSS download, positioning and analysis, which is developed by GNSS Analysis Center, Shanghai Astronomical Observatory, Chinese Academy of Sciences and supports both desktop and online versions (Chen et al., 2020; Zhang et al., 2020). The details of how this actually works can refer to the website (http://202.127.29.4/shao_gnss_ac/Net_diff/Net_diff.html). As for SF-SPP, both satellite orbits and clock offsets are corrected by the broadcast ephemeris. Due to the difference of signal in space range error (SISRE) accuracy between different GNSS, a proper stochastic model provided by Zhang et al. (2019b) is adopted in this processing. Concerning SF-PPP, the RT precise orbit and clock offset products are used, which are computed from the CLK93 orbit and clock corrections as well as the broadcast ephemeris (Elsobeiey and Al-Harbi, 2016; Kazmierski et al., 2018a). The standard deviation of code and phase observations for GPS and Galileo is set to 0.3 m and 0.003 m, respectively. According to the precision of RT orbit and clock from the CLK93 stream in Section 4.1, the standard deviation of observations for GLONASS is set as twice as that of GPS, while for BDS IGSO (Inclined Geosynchronous Orbit)/MEO (Medium Earth Orbit), its standard deviation is set as four times as that of GPS. Noted that BDS GEO (Geostationary Earth Orbit) satellites are excluded in this experiment as the corresponding accuracy of their RTS products is too low to meet the demands of SF-PPP (Wang et al., 2018; Cao et al., 2018). Adopted models and process strategies for multi-GNSS SF-SPP/PPP are presented in Table 1. In this study, SF1 and SF2 are used to represent observations on the first and the second frequency to keep the consistency of both code and phase observations for quad-constellation.

4. Quality assessment of CNES CLK93 products

4.1. RTS orbits and clock offsets

The BNC (BKG NTRIP Client, https://igs.bkg.bund.de/ntrip/download) software is utilized to receive and decode the RTS corrections from the CLK93 stream for 14 consecutive days (from April 27, 2019, to May 10,

Table 1
Adopted models and strategies for multi-GNSS single-frequency SPP/PPP.

Item	Models/Strategies
Frequency selection	GPS: L1C/L2W; GLONASS: L1C/L2C; BDS: L2I/L7I; Galileo: L1C/L5X
Sampling rate	30 s
Elevation cutoff angle	10°
Estimator	SPP: Least squares PPP: Kalman filter
Weighing strategy	Elevation-dependent weighing model
Tropospheric delay	Modified (GPT2w + SAAS + VMF (Boehm et al. 2015)) for the dry part and estimated for the wet part as a random-walk noise process
Ionospheric delay	SPP: Corrected using CNES VTEC products PPP: Estimated as a random-walk noise process
Receiver antenna phase center	PCO (phase center offset)/PCV (phase center variation) values for GPS and GLONASS from igs14.atx are used; Corrections for BDS and Galileo are assumed the same with GPS
Satellite antenna phase center	PCO/PCV values for GPS, GLONASS and Galileo from igs14.atx are used; BDS PCO corrected with the value released by ESA and PCV is not considered
Timing group delay	SPP: Correct using broadcast ephemeris
Differential code bias	PPP: Correct using CLK93 bias products
Tidal effects	Consider solid tides, ocean loading tides and polar tides (Gerard and Luzum, 2010)
Other corrections	Considering phase windup, relativistic and earth rotation effects
Station reference coordinates	IGS weekly SINEX solutions
Station coordinates	SPP/PPP: estimated as white noises
Receiver clock	Estimated as white noise process
Receiver ISB	Set up for GLONASS/BDS/Galileo and estimated as a random-walk noise process (Zhou et al., 2019)
GLONASS code IFB	Modeled as a linear function of channel numbers
Phase ambiguities	Estimated as a constant parameter if no cycle slip occurs

2019). Since the RTS data interruption is caused by loss of network connection, the mean availability of CLK93 products for quad-constellation is about 95.25% during the test period. When the RTS orbits are missing, the most updated IGS Ultra-rapid (IGU) orbits are used as an alternative since they have the same accuracy (EI-Mowafy et al., 2017). As to RTS clock offsets, however, the IGU predicted part cannot work well in RT-PPP. Hence, the missing RTS clock corrections can be predicted by polynomial fitting with the recorded RTS clock corrections in a short time (Hadas and Bosy, 2015). According to the standard of RTCM (Radio Technical Commission for Maritime Services)-SSR, the RTS orbit and clock corrections are combined with broadcast ephemeris to generate the RT precise products. The details of the matching algorithm can refer to the following literature (Hadas and Bosy, 2015; Kazmierski et al., 2018a; Cao et al., 2018).

In order to evaluate the quality of RTS orbits and clock offsets for quad-constellation, the final precise products of GBM released by Deutsches GeoForschungsZentrum (GFZ; Deng et al., 2016) were employed as references. The orbit comparison was performed every 5 min for the radial, along-track and cross-track components. Clock offsets were compared every 30 s in terms of the interval provided by the final high-rate clock products. The triple times of standard deviations (SD) of the analyzed datasets as a threshold is used to remove outliers in this contribution (Kazmierski et al., 2018a). It is worth noting that the CLK93 stream refers to the satellite antenna phase center (APC) whereas the GBM final products directly adopt the center of mass (CoM) of the satellite, thus the phase center offset (PCO) correction must be taken into account. With regard to satellite clock, broadcast ephemeris (i.e., CLK93 products) exhibits small offsets from each satellite because it refers to constellation-specific timescale, while precise ephemeris (i.e., GBM products) applies a product-specific timescale. The difference between the aforementioned two ephemerides is generally unknown but common to all satellites of a constellation. It must be excluded from the assessment of real-time clock by adjusting an epoch-wise average CLK93-minus-GBM clock value of all satellites for one constellation (Montenbruck et al., 2018). To avoid the influence of gross error from some satellites, a medium value of CLK93-minus-GBM clock at each epoch is computed as the ensemble clock difference to remove this systematic bias (Zhang et al., 2019b).

Fig. 2 shows the satellite-specific RMS of differences in the radial, along-track and cross-track components as well as clock offsets between the CLK93 products and the GBM final products. For each GNSS, their mean RMS values over all satellites are also presented in Table 2. Generally, the orbit accuracy of each system in the radial component is much better than that in both along-track and cross-track components. The quality of GPS orbits and clock offsets is the best, its accuracy is better than 4 cm in all orbit components and 0.3 ns in the clock errors. The Galileo has slightly worse accuracy than GPS, with the mean RMS of orbit and clock errors being less than 5 cm and 0.4 ns, respectively, which are close to the results as reported by Kazmierski et al. (2018b). For GLONASS, the orbit accuracy is about 4.2, 11.6 and 7.3 cm, respectively, in the radial, alone-track and cross-track components,

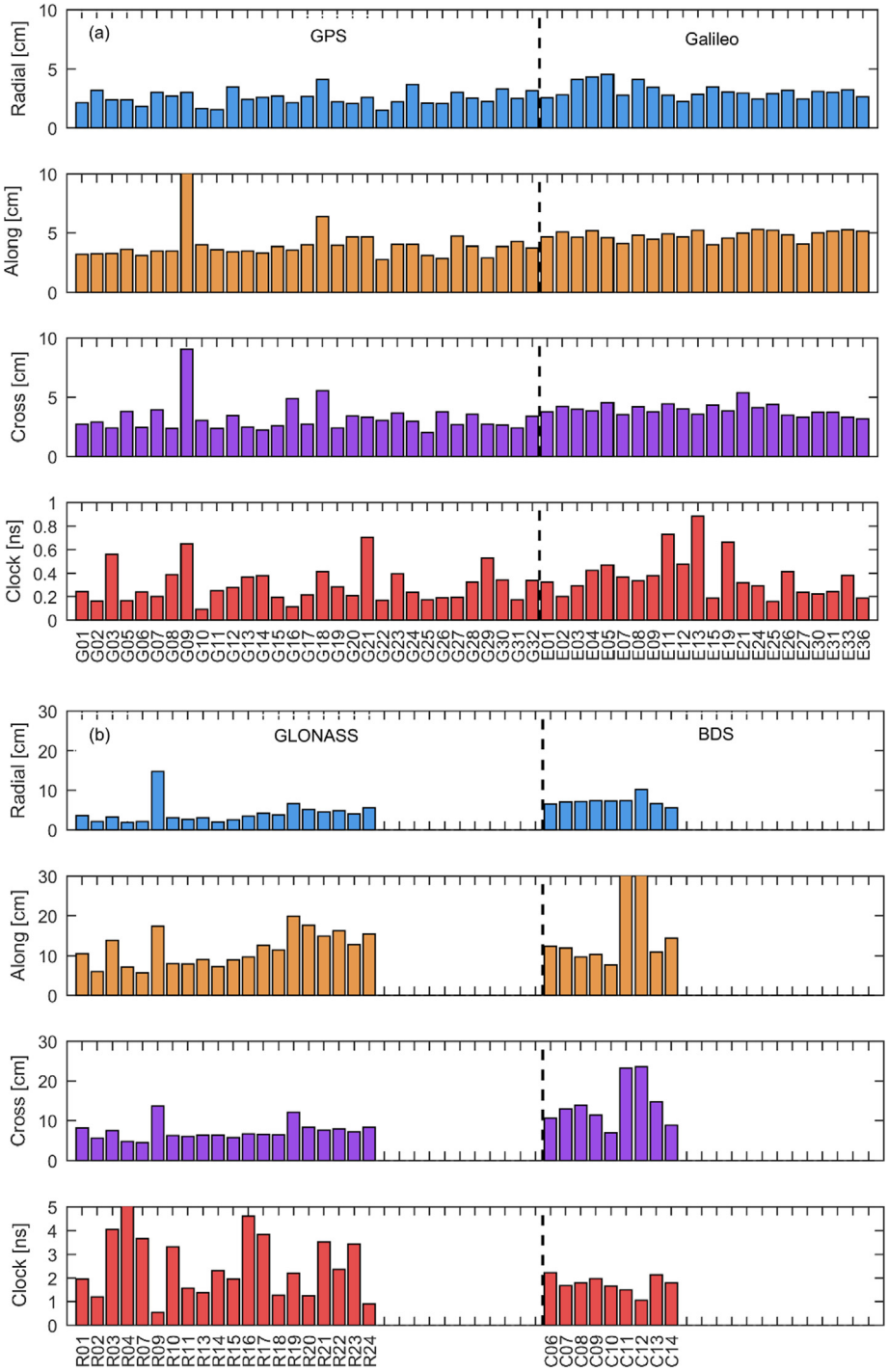

Fig. 2. The RMS values of the differences between orbits and clock offsets calculated based on CLK93 products regarding GBM final products during DoYs 117–130, 2019.

which is about twice worse than of GPS. However, there is an exception for GLONASS-K R09 satellite, whose radial accuracy is up to 19.5 cm. As to clock accuracy, the RMS of GLONASS is about 2.5 ns, which is much higher than other systems. BDS satellites (C06-C14) have the worst orbit performance among all GNSS and its mean RMS in radial, along-track and cross-track components are individually 7.3, 16.2 and 14.1 cm. Regarding the accuracy of the BDS clock, the mean RMS value is 1.76 ns, which is much worse than GPS and Galileo since the number of contributed ground stations that can track BDS satellites is insufficient. The results of BDS satellite orbit and clock are almost the same accuracy as those indicated by Wang et al. (2018).

4.2. Real-time VTEC products

Since the prior ionosphere constrains is applied to the STEC rather than VTEC, the quality of STEC (Slant Total

Table 2
The averaged RMS values of CLK93 orbit errors in the radial (R), along-track (A) and cross-track (C) components as well as clock errors (T) in a 14-day test period.

Constellation	R (cm)	A (cm)	C (cm)	3D (cm)	T (ns)
GPS	2.57	3.98	3.24	5.73	0.29
GLONASS	4.20	11.59	7.28	14.31	2.52
BDS	7.26	16.20	14.05	22.63	1.76
Galileo	3.14	4.81	3.93	6.96	0.37

Electron Content) derived from the CNES VTEC products should be evaluated. Compared with Liu et al. (2018), which only shows one-day STEC precision of GPS/Galileo satellites for one station, 46 globally distributed MGEX stations (Fig. 1) and the GPS + GLONASS + BDS + Gali leo observations with a sample rate of 30 s in 14 days (DoY 117–130 in 2019) are used to calculate the STEC in this study. Noted that the CNES VTEC is based on the 12-degree and 12-order of the spherical harmonic function. The referenced STEC derived from a post-processing GIM product from CODE (Center for Orbit Determination in Europe) agency because it has the highest accuracy in all ACs (Cai et al., 2017). In the test period, the solar activity and ionosphere variation are relatively mild as the radio flux index F10.7 is no more than 80 sfu and the most of geomagnetic Kp index is less than 3 (Fig. 3).

The bias and RMS values of the CNES STEC for 46 stations during the testing are shown in the Fig. 4. The bias value varies from −4.46 to 2.85 TECU, and the averaged bias of all selected MGEX stations is −0.72 TECU. As for RMS, the average value for all stations is 3.43 TECU. The maximum RMS of 5.9 TECU comes from low latitude (22.4°N) MGEX station HKSL, which is located in Southeast China, and the minimum RMS is derived from high latitude (67.9°N) MGEX station KIRO at 1.44 TECU. In

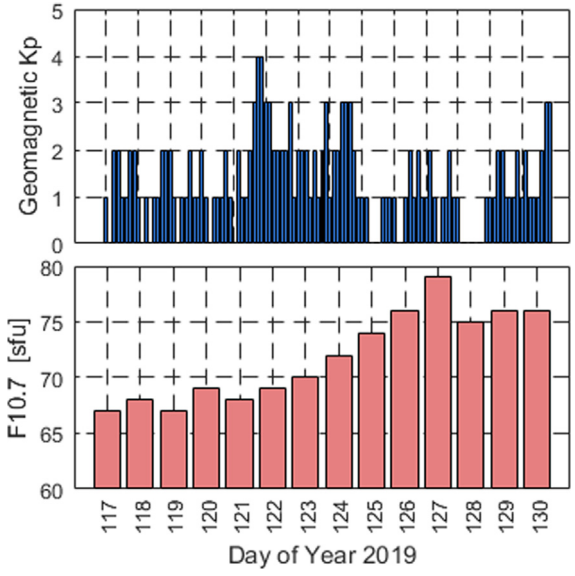

Fig. 3. Geomagnetic Kp index and F10.7 values during DoYs 117–130, 2019.

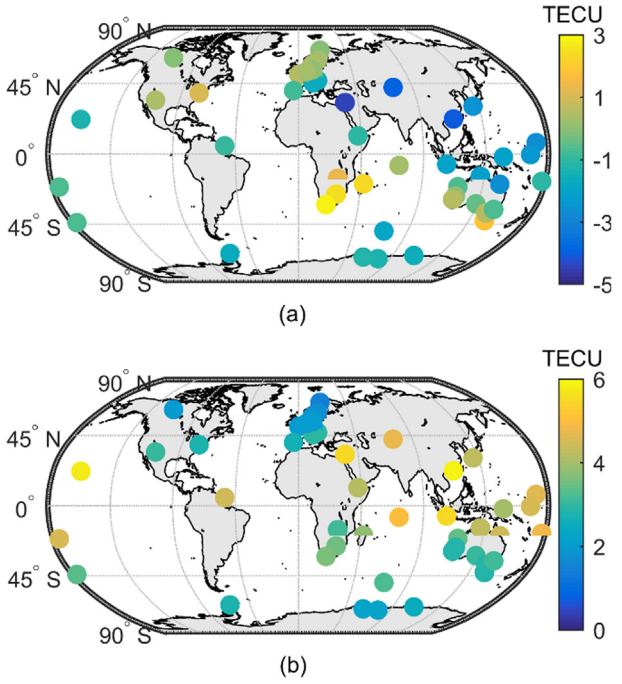

Fig. 4. The (a) bias and (b) RMS values of the CNES STEC for 46 MGEX stations during a 14-day test period.

general, the accuracy of the CNES STEC for low latitude stations is worse than middle and high latitude stations, which accords with a feature of any ionospheric model (Rovira-Garcia et al., 2020). On the other hand, the stations located in ocean areas such as KOKB and TONG show relatively larger RMS computed from the CNES STEC. The main reason is that the ionospheric properties cannot be accurately described by the global spherical harmonic function model because of the sparse reference stations in these areas.

5. Performance analysis of real-time single-frequency positioning

5.1. Single-frequency SPP

To investigate the performance of CNES VTEC products on the multi-GNSS SF-SPP, the high-precision global ionosphere product from the CODE agency as the reference is also applied to the same positioning processing, which means that only the external ionospheric models used in SF-SPP e different. Fig. 5 depicts the SF1 epoch-wise positioning errors of HARB station on 27 April 2019 for the south-north (N), west-east (E) and up (U) components based on the ionospheric delay correction of CNES VTEC products (i.e. CLK93-VTEC) and CODE-GIM. It can be seen that the single- and multi-system SF-SPP results with CLK93-VTEC and CODE-GIM products perform similarly. The vertical error of SF-SPP with broadcast ephemeris is relatively larger than that of horizontal error and can achieve meter-level. Due to the

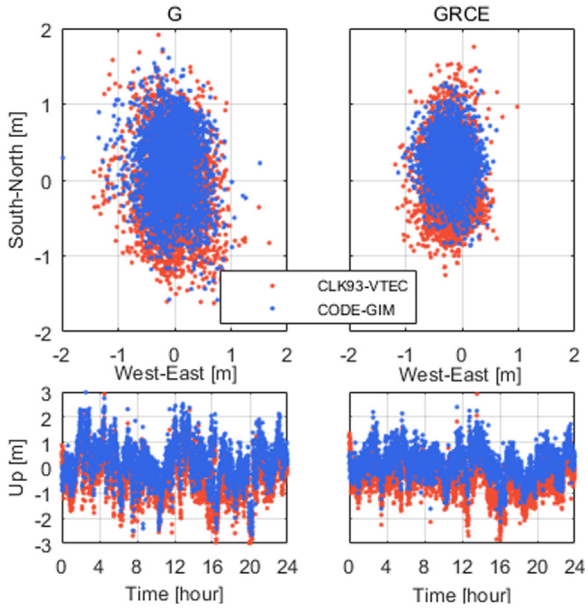

Fig. 5. Positioning errors of SF1 SF-SPP with two types of ionospheric products (CLK93-VTEC and CODE-GIM) in (a) single-system or (b) multi-system at HARB station (DoY 117 in 2019). The abbreviation G, R, C and E denote GPS, GLONASS, BDS, Galileo, respectively.

improved satellite geometry of multi-GNSS, the positioning accuracy of SF-SPP with quad-constellation in both horizontal and vertical components is better than that of GPS-only.

The RMS statistics in the N, E, U and three-dimensional (3D) positioning errors in different SF-SPP solutions on all days of all the selected stations are summarized in Table 3. For all single-system SF-SPP solutions, the performance of GPS-only and Galileo-only is at the same level and much better than the other systems, which is mainly attributed to the higher accuracy of broadcast orbits and clocks. Although GLONASS currently has the smaller position dilution of precision (PDOP) than BDS, its positioning accuracy is still worse than that of BDS. The main reason is that the GLONASS code observation has a higher measurement noise level (Montenbruck, 2003) and the IFB is neglected in SPP. Fig. 6 shows the mean PDOP of SF1 and SF2 BDS-only SF-SPP at all selected stations, but stations with mean PDOP more than 6 are excluded. As for BDS-2, tri-frequency signals (B1/B2/B3) can be received by the 46 selected MGEX stations, while for BDS-3, only observations of B1 and B3 can be tracked. Therefore, the number of B2 tracked satellites is less than that of B1 for BDS-2 + 3 during the test period. The satellite geometry of SF1 BDS-only with the introduction of BDS-3 satellites is much better than that of SF2, which results in better positioning accuracy of SF1 solution.

For the multi-GNSS SF-SPP, the performance of GPS + GLONASS + BDS + Galileo with CODE-GIM correction shows the best, in which the positioning accuracy of the horizontal and vertical components is better than 0.7 m and 1.5 m, respectively. One reason is that the PDOP is smallest with the increased number of visible satellites, another is that the CODE-GIM as the post-processed product has higher accuracy than RT models. However, compared with the CODE-GIM correction, for the single- or multi-system users, the 3D positioning accuracy of SF-SPP with CLK93-VTEC correction is only reduced by no more than 7%, which is mainly reflected in the N direction. It should be noted that the errors of broadcast orbits and clocks and the pseudorange noise used in SPP are interfering with the results of the assessment of ionospheric models. During the period of mild solar activity, the CNES VTEC products can substitute for the final GIM products in SF-SPP considering the meter-level positioning accuracy requirements. Besides, whether this

Table 3
RMS values of SF-SPP with CLK93-VTEC and CODE-GIM based ionospheric delay correction for SF1 and SF2 (unit: m). SF1 and SF2 are used to represent results on the first and the second frequency.

System	Iono-Corr	SF1				SF2			
		N	E	U	3D	N	E	U	3D
G	CLK93-VTEC	0.819	0.624	1.481	1.804	1.094	0.764	1.838	2.272
G	CODE-GIM	0.684	0.577	1.470	1.721	0.820	0.658	1.856	2.133
R	CLK93-VTEC	2.389	2.518	4.470	5.659	2.250	2.226	4.271	5.316
R	CODE-GIM	2.357	2.510	4.475	5.646	2.154	2.210	4.273	5.271
C	CLK93-VTEC	1.264	1.402	2.485	3.121	1.899	2.419	3.540	4.689
C	CODE-GIM	1.138	1.372	2.410	2.997	1.726	2.373	3.518	4.580
E	CLK93-VTEC	0.718	0.553	1.352	1.627	1.138	0.839	1.993	2.443
E	CODE-GIM	0.572	0.513	1.344	1.548	0.871	0.747	2.004	2.309
GR	CLK93-VTEC	0.791	0.601	1.432	1.743	1.039	0.718	1.710	2.125
GR	CODE-GIM	0.657	0.560	1.423	1.664	0.772	0.626	1.755	2.017
GC	CLK93-VTEC	0.756	0.567	1.344	1.643	1.054	0.719	1.721	2.142
GC	CODE-GIM	0.601	0.521	1.317	1.538	0.765	0.626	1.758	2.016
GE	CLK93-VTEC	0.681	0.500	1.196	1.464	0.995	0.657	1.610	2.003
GE	CODE-GIM	0.520	0.451	1.182	1.368	0.695	0.551	1.653	1.876
GRCE	CLK93-VTEC	0.649	0.469	1.112	1.370	0.938	0.620	1.454	1.838
GRCE	CODE-GIM	0.483	0.419	1.097	1.270	0.647	0.519	1.499	1.713

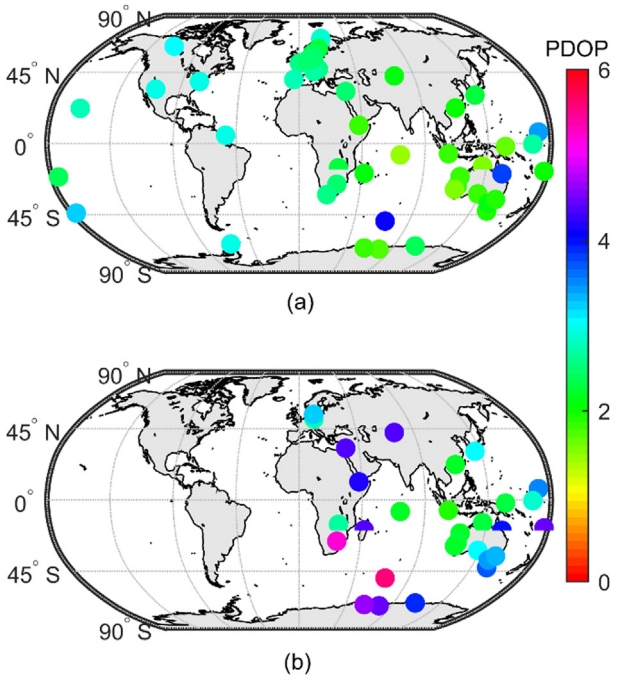

Fig. 6. Mean PDOP of BDS-only SF-SPP at (a) 46 SF1 MGEX stations and (b) 29 SF2 MGEX stations during DoYs 117–130, 2019.

finding is applicable to low latitudes areas or high solar activity period needs further study.

5.2. Kinematic RT-SF-PPP

To compare the kinematic positioning performance between the GRAPHIC and CLK93-VTEC-constrained models, the multi-GNSS observations from GRAZ station on 5 May 2019 are selected for the test. Fig. 7 presents the positioning errors of SF1 kinematic RT-SF-PPP with different schemes. It is obvious that the time series of the CLK93-VTEC-constrained model is smoother than that of the GRAPHIC model. By introducing the multi-GNSS observations, the improvement of positioning accuracy is mainly reflected in the vertical component, whereas the horizontal component has little change.

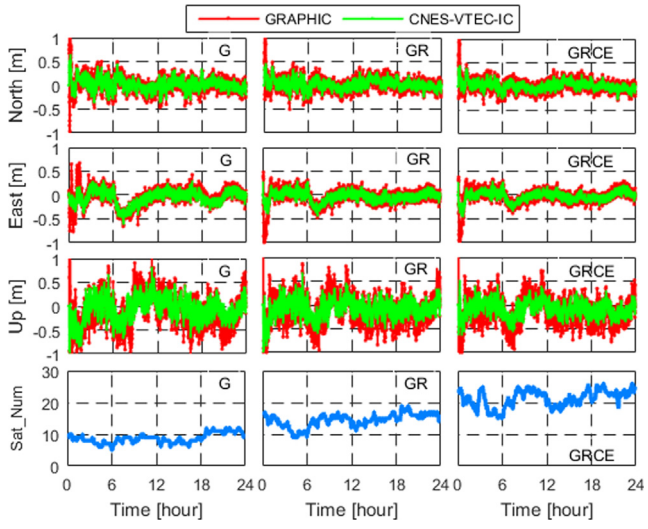

Fig. 7. Comparison of positioning errors of SF1 kinematic RT-SF-PPP with different models for single- or multi-system at GRAZ station (DoY 125 in 2019). The corresponding number of satellites is represented by the blue curve. (For interpretation of the references to colour in this figure legend, the reader is referred to the web version of this article.)

Fig. 8 shows the RMS values of 3D positioning errors of SF1 kinematic RT-SF-PPP with different schemes for 46 globally distributed MGEX stations. Noted that the results of GPS + BDS are not shown in Fig. 8 due to its performance is basically the same as GPS-only. In the GRAPHIC model, the 3D positioning accuracy of 32 stations for GPS-only exceeds 0.5 m, whereas, for the quad-constellation, the amount of stations is reduced to 14. By adopting the CLK93-VTEC-constrained model, the accuracy of almost all stations for single- or multi-system has been improved to some extent, and there are 42 stations with a 3D positioning accuracy of less than 0.5 m for RT-SF-PPP with quad-constellation. From the results of GPS-only with CLK93-VTEC-constrained, the positioning accuracy of the stations in the adjacent sea area is relatively poor, which is probably caused by the quality degradation of CLK93-VTEC products over the areas lacking observations.

Table 4 summarizes the RMS values of positioning errors of RT-SF-PPP with different schemes. It should be noted that the statistical result is computed from the converged epoch to the last epoch of a day, and the conver-

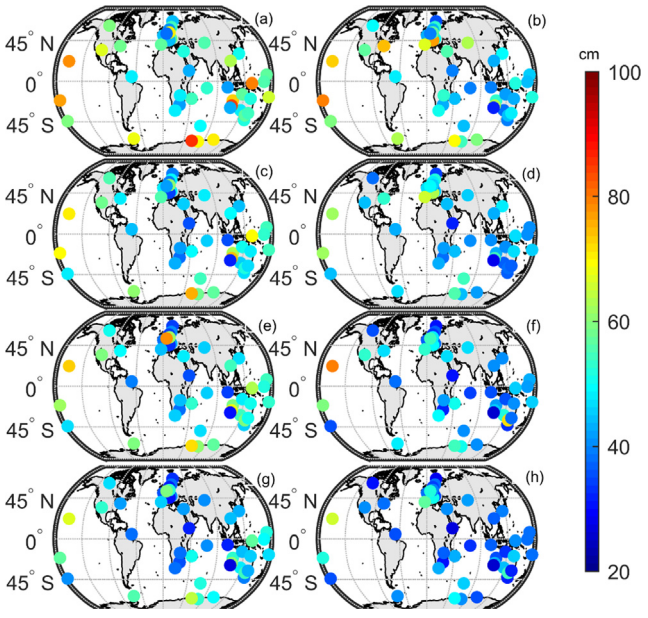

Fig. 8. RMS values of 3D positioning errors of SF1 kinematic RT-SF-PPP with different models during the period of DoYs 117–130, 2019. (a) GPS-only GRAPHIC, (b) GPS-only CLK93-VTEC-constrained, (c) GPS + GLONASS GRAPHIC, (d) GPS + GLONASS CLK93-VTEC-constrained, (e) GPS + Galileo GRAPHIC, (f) GPS + Galileo CLK93-VTEC-constrained, (g) GPS + GLONASS + BDS + Galileo GRAPHIC, (h) GPS + GLONASS + BDS + Galileo CLK93-VTEC-constrained.

Table 4
RMS values of kinematic RT-SF-PPP with the GRAPHIC and CLK93-VTEC-constrained models for SF1 and SF2 (unit: cm).

System	Iono-Corr	SF1				SF2			
		N	E	U	3D	N	E	U	3D
G	CLK93-VTEC	21.1	25.8	40.4	52.3	21.5	24.9	39.6	51.4
G	GRAPHIC	23.3	23.4	48.0	58.3	24.7	26.3	48.1	60.1
GR	CLK93-VTEC	19.6	23.6	35.6	47.0	19.5	22.6	35.4	46.3
GR	GRAPHIC	21.4	21.5	43.4	52.9	21.6	21.7	41.1	51.3
GC	CLK93-VTEC	21.4	26.3	40.6	52.9	21.1	25.4	38.1	50.5
GC	GRAPHIC	23.1	23.2	47.6	57.8	24.5	26.1	47.7	59.6
GE	CLK93-VTEC	20.2	22.9	35.3	46.7	18.6	21.0	34.3	44.3
GE	GRAPHIC	20.5	20.7	42.0	51.1	21.9	22.9	41.7	52.4
GRCE	CLK93-VTEC	18.8	21.7	31.9	42.9	17.9	19.8	32.2	41.8
GRCE	GRAPHIC	18.9	19.1	38.5	47.0	19.7	20.0	37.3	46.6

gence criterion for 3D positioning errors is set to 1.5 m. Typically, using both GRAPHIC or CLK93-VTEC-constrained model, the positioning accuracy of 0.3 m in horizontal and 0.5 m in vertical can be achieved in the GPS-only RT-SF-PPP in our study. As for the results of Nie et al. (2019), the horizontal and vertical positioning accuracy of the traditional SF-PPP (i.e., ionosphere-corrected model) using the CNES VTEC products is 0.7 m and 1.0 m, respectively. Thus, our results are twice better than that of Nie et al. (2019). The main reason is that the ionospheric errors in the ionosphere-corrected SF-PPP model are only partially mitigated by the CNES VTEC products and the residual of ionospheric errors still has some effect on the position accuracy, whereas the residual of ionospheric errors has been removed by estimating them as parameters or using a GRAPHIC model in our contribution. With the combination of multi-GNSS observations, the 3D positioning accuracy of GPS + GLONASS + BDS + Galileo SF2 RT-SF-PPP based on the GRAPHIC and CLK93-VTEC-constrained model is improved by 22.46% and 18.68%, respectively, compared with the GPS-only. On the other hand, compared with the GRAPHIC model, the improvement in 3D positioning accuracy of CLK93-VTEC-constrained RT-SF-PPP with quad-constellation for SF1 and SF2 is 8.72% and 10.30%, respectively. The main reason is that the GRAPHIC combination introduces half of the code noise, which is much larger than the phase noise in the CLK93-VTEC-constrained model (Li et al., 2020). To summarize, the CLK93-VTEC-constrained GPS + GLONASS + BDS + Galileo RT-SF-PPP has the best positioning performance, which RMS in N, E and U components can reach 17.9, 19.8 and 32.3 cm, respectively. It should be noted that the simulated kinematic positioning using MGEX static data is under an ideal situation and theoretically better than true real-time applications.

The (re-)convergence time is a key indicator of the RT kinematic PPP. In order to present the (re-)convergence difference between the IF and IC models, the simulated signal interruptions are introduced every 4 h by adding a new set of ambiguities for all used satellites, while all other estimated parameters are kept in the positioning filter with their covariances from the previous epoch (Shi et al., 2012). Taking the GPS + GLONASS + BDS + Galileo data from GRAZ station on 5 May 2019 as an example, the convergence performance of the abovementioned two RT-SF-PPP models is compared and shown in Fig. 9. From the position time series on the top panel of Fig. 9, the positioning errors of the GRAPHIC model after each interruption is visibly much worse and need around 20–30 min to (re-)convergence. However, the CLK93-VTEC-constrained model has almost no obvious discontinuity in the whole time series. Compared with the first convergence, the re-convergence can be accelerated significantly as expected (Shi et al., 2012). The major reason is that the ionospheric effect is adequately compensated by applying proper priori constraints in the CLK93-VTEC-constrained model. Therefore, the CLK93-VTEC-constrained kinematic RT-SF-PPP has a great advantage in (re-)convergence and should be recommended.

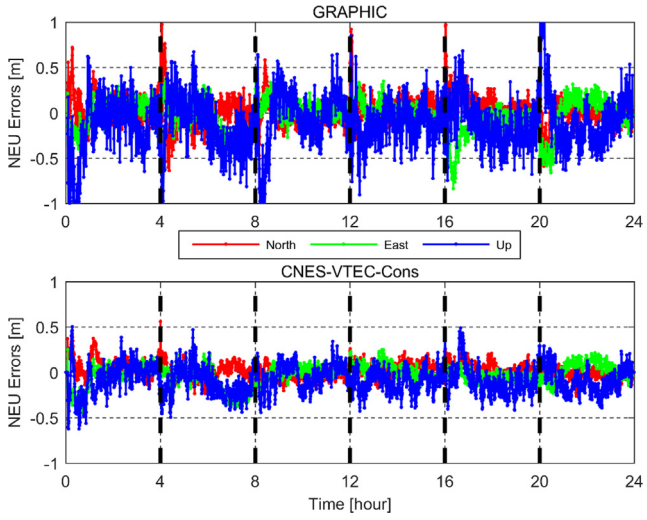

Fig. 9. Positioning errors of SF1 kinematic RT-SF-PPP in the North, East and Up components for GRAZ station (DoY 125 in 2019). The top panel shows the results of the GRAPHIC model and the bottom for that of the CLK93-VTEC-constrained model.

6. Conclusions

Single-frequency GNSS receivers play an important role in most fields of PNT due to their low costs and high-precision. With the increasing demand for RT applications, the RT-SF-SPP/PPP technique has attracted more and more attention in the GNSS market. Typically, the performance of RT single-frequency positioning is seriously affected by the low precision of several existing broadcast ionospheric models such as Klobuchar. However, since the release of the CNES VTEC products through SSR messages from CLK93, this situation has begun to improve.

In this contribution, we focus on evaluating the impact of CNES VTEC products on multi-GNSS RT SF-SPP/PPP performance. The CLK93 corrections and the observations of 46 globally distributed MGEX stations for 14 consecutive days were selected to process with different positioning scenarios. Compared with the final precise products of GBM, the satellite orbit accuracy of CLK93 products is 4, 5, 12 and 16 cm for GPS, Galileo, GLONASS and BDS, respectively. As for the CLK93 satellite clock, its RMS accuracy of GPS, Galileo, GLONASS and BDS is 0.3, 0.4, 2.5 and 1.8 ns, respectively.

The results of positioning experiments strongly demonstrated the following conclusions. The single- and multi-GNSS kinematic SF-SPP with CNES VTEC correction is comparable with positioning accuracy based on the final GIM products in mild solar activity period, and its slight differences are mainly reflected in the N component. Statistical results indicated that the positioning accuracy of GPS + GLONASS + BDS + Galileo SF-SPP with CNES VTEC correction is better than 1.0 m and 1.5 m in the horizontal and vertical components, respectively. Regarding the kinematic RT-SF-PPP, the (re-)convergence can be accelerated by adopting an appropriate ionosphere information. Since the GRAPHIC observations are affected by the code noise, the positioning accuracy is slightly worse than that of the CNES-VTEC-constrained model. For the GPS + GLONASS + BDS + Galileo users, the improvement in positioning accuracy of SF1 and SF2 CNES-VTEC-constrained kinematic RT-SF-PPP is 8.72% and 10.30%, respectively, compared with the GRAPHIC model. The best positioning accuracy of kinematic RT-SF-PPP can be achieved by introducing the quad-constellation observations and CNES VTEC products, in which the average RMS is 17.9, 19.8 and 32.3 cm in the N, E and U components, respectively. Furthermore, the impact of the CNES real-time VTEC products on multi-GNSS single-frequency positioning in high solar activity will be evaluated in future works.

Declaration of Competing Interest

None.

Acknowledgments

This research is supported by the National Natural Science Foundation of China (No.11673050); the Key Program of Special Development funds of Zhangjiang National Innovation Demonstration Zone (Grant No. ZJ2018-ZD-009); the National Key R&D Program of China (No.2018YFB0504300); and the Key R&D Program of Guangdong province (No.2018B030325001). We sincerely thank the IGS and its Multi-GNSS Experiment for the provision of broadcast ephemeris and observation data. The effort of IGS RTS is very appreciated for providing real-time orbit corrections, clock corrections and VTEC messages.

References

Bidaine, B., 2012. Ionosphere modelling for Galileo single frequency users Ph.D thesis. University of Liege, Liege, Belgium.

Boehm, J., Moller, G., Schindelegger, M., Pain, G., Weber, R., 2015. Development of an improved empirical model for slant delays in the troposphere (GPT2w). GPS Solut. 19, 433–441.

Cai, C., Liu, Z., Luo, X., 2013. Single-frequency ionosphere-free precise point positioning using combined GPS and GLONASS observations. J. Navig. 66 (3), 417–434.

Cai, C., Gong, Y., Gao, Y., Kuang, C., 2017. An approach to speed up single-frequency PPP convergence with quad-constellation GNSS and GIM. Sensors 17, 1302.

Cao, X., Li, J., Zhang, S., Pan, L., Kuang, K., 2018. Performance assessment of uncombined precise point positioning using multi-GNSS real-time streams: computational efficiency and RTS interruption. Adv. Space Res. 62, 3133–3147.

Chen, J., Wang, A., Zhang, Y., Zhou, J., Yu, C., 2020. BDS satellite-based augmentation service correction parameters and performance assessment. Remote Sens. 12, 766.

Choy, S., Zhang, K., Silcock, D., 2008. An evaluation of various ionospheric error mitigation methods used in single-frequency PPP. Positioning 7 (1), 62–71.

de Bakker, P.F., Tiberius, C.C.J.M., 2017. Real-time multi-GNSS single-frequency precise point positioning. GPS Solut. 21, 1791–1803.

Deng, Z., Fritsche, M., Uhlemann, M., 2016. Reprocessing of GFZ multi-GNSS product GBM. IGS Workshop 2016, Sydney.

EI-Mowafy, A., Deo, M., Kubo, N., 2017. Maintaining real-time precise point positioning during outages of orbit and clock corrections. GPS Solut. 21 (3), 937–947.

Elsobeiey, M., Al-Harbi, S., 2016. Performance of real-time precise point positioning using IGS real-time service. GPS Solut. 20, 565–571.

Feess, W., Stephens, S., 1987. Evaluation of GPS ionospheric time-delay model. Aerosp. Electron. Syst. IEEE Trans. 3, 332–338.

Gerard, P., Luzum, B., 2010. IERS Conventions. IERS Technical 2010 Note 36. Verlag des Bundesamts für Kartographie und Geodäsie, Frankfurt am Main,Germany, 2010.

Hadas, T., Bosy, J., 2015. IGS RTS precise orbits and clocks verification and quality degradation over time. GPS Solut. 19 (1), 93–105.

Hoque, M., Jakowski, N., 2015. An alternative ionospheric correction model for global navigation satellite systems. J. Geod. 89 (4), 391–406.

Jin, S., Qian, X., Wu, X., 2017. Sea level change from BeiDou Navigation Satellite System-Reflectometry (BDS-R): first results and evaluation. Global Planet. Change 149, 20–25.

Juan, J.M., Hernandez-Pajares, M., Sanz, J., Ramos-Bosch, P., Aragon-Angel, A., Orus, R., Ochieng, W., Feng, S., Jofre, M., Coutinho, P., Samson, J., Tossaint, M., 2012. Enhanced precise point positioning for GNSS users. IEEE Trans. Geosci. Remote Sens. 50, 4213–4222.

Kazmierski, K., Sosnica, K., Hadas, T., 2018a. Quality assessment of multi-GNSS orbits and clocks for real-time precise point positioning. GPS Solut. 22, 11.

Kazmierski, K., Hadas, T., Sosnica, K., 2018b. Weighting of multi-GNSS observations in real-time precise point positioning. Remote Sens. 10, 84.

Klobuchar, J., 1987. Ionospheric time-delay algorithm for single-frequency GPS users. IEEE Trans. Aerosp. Electron. Syst. 23, 325–331.

Kouba, J., Heroux, P., 2001. Precise point positioning using IGS orbit and clock products. GPS Solut. 5 (2), 12–28.

Liu, T., Wang, J., Yu, H., Cao, X., Ge, Y., 2018. A new weighting approach with application to ionospheric delay constraint for GPS/GALILEO real-time precise point positioning. Appl. Sci. 8, 2537.

Liu, Z., Yang, Z., 2016. Anomalies in broadcast ionospheric coefficients recorded by GPS receivers over the past two solar cycles (1992–2013). GPS Solut. 20, 23–37.

Li, B., Zang, N., Ge, H., Shen, Y., 2020. Single-frequency PPP models: analytical and numerical comparison. J. Geod. 93, 2499–2514.

Li, X., Zhang, X., Ge, M., 2011. Regional reference network augmented precise point positioning for instantaneous ambiguity resolution. J. Geod. 85 (3), 151–158.

Li, X., Ge, M., Zhang, H., Wickert, J., 2013. A method for improving uncalibrated phase delay estimation and ambiguity-fixing in real-time precise point positioning. J. Geod. 87 (5), 405–416.

Li, X., Ge, M., Dai, X., Ren, X., Fritsche, M., Wickert, J., Schuh, H., 2015. Accuracy and reliability of multi-GNSS real-time precise positioning: GPS, GLONASS, BeiDou, and Galileo. J. Geod. 89, 607–635.

Montenbruck, O., 2003. Kinematic GPS positioning of LEO satellites using ionosphere-free single frequency measurements. Aerosp. Sci. Technol. 7, 396–405.

Montenbruck, O., Steigenberger, P., Hauschild, A., 2018. Multi-GNSS signal-in-space range error assessment – methodology and results. Adv. Space Res. 61 (12), 3020–3038.

Nie, Z., Yang, H., Zhou, P., Gao, Y., Wang, Z., 2019. Quality assessment of CNES real-time ionospheric products. GPS Solut. 23, 11.

Odolinski, R., Teunissen, P.J.G., 2017. Low-cost, high-precision, single-frequency GPS-BDS RTK positioning. GPS Solut. 21, 1315–1330.

Roma, D., Hernandez, M., Garcia-Rigo, A., Laurichesse, D., Schmidt, M., Erdogan, E., Yuan, Y., Li, Z., Gomez-Cama, J.M., Krankowski, A., 2016. Real time global ionospheric maps: a low latency alternative to traditional GIMs. 19th International Beacon Satellite Symposium (BSS 2016).

Rovira-Garcia, A., Ibanez-Segura, D., Orus-Perez, R., Juan, J.M., Sanz, J., Gonzalez-Casado, G., 2020. Assessing the quality of ionospheric models through GNSS positioning error: methodology and results. GPS Solut. 24, 4.

RTCM Special Committee, 2016. RTCM Standard 10403.3 differential GNSS (Global Navigation Satellite Systems) Services-Version 3. RTCM Special Committee No.104, Arlington, TX, USA.

Shi, C., Gu, S., Lou, Y., Ge, M., 2012. An improved approach to model ionospheric delays for single-frequency precise point positioning. Adv. Space Res. 49, 1698–1708.

Torre, A.D., Caporali, A., 2015. An analysis of intersystem biases for multi-GNSS positioning. GPS Solut. 19, 297–307.

van Bree, R.J.P., Tiberius, C.C.J.M., 2012. Real-time single-frequency precise point positioning: accuracy assessment. GPS Solut. 16, 259–266.

Wanninger, L., 2012. Carrier-phase inter-frequency biases of GLONASS receivers. GPS Solut. 86, 139–148.

Wang, A., Chen, J., Zhang, Y., Meng, L., Wang, J., 2019a. Performance of Selected Ionospheric Models in Multi-Global Navigation Satellite System Single-frequency Positioning over China. Remote Sens. 11, 2070.

Wang, M., Wang, J., Bock, Y., Liang, H., Dong, D., Fang, P., 2019b. Dynamic mapping of the movement of landfalling atmospheric rivers over southern California with GPS data. Geophys. Res. Lett. 46.

Wang, Z., Li, Z., Wang, L., Wang, X., Yuan, H., 2018. Assessment of multiple GNSS real-time SSR products from different analysis centers. ISPRS Int. J. Geo-Inf. 7, 85.

Wu, X., Hu, X., Wang, G., Zhou, H., Tang, C., 2013. Evaluation of COMPASS ionospheric model in GNSS positioning. Adv. Space Res. 51 (6), 959–968.

Yuan, Y., Wang, N., Li, Z., Huo, X., 2019. The BeiDou global broadcast ionospheric delay correction model (BDGIM) and its preliminary performance evaluation results. Navigation 66 (1), 55–69.

Zhang, H., Gao, Z., Ge, M., Niu, X., Huang, L., Tu, R., Li, X., 2013. On the convergence of ionospheric constrained precise point positioning (IC-PPP) based on undifferential uncombined raw GNSS observations. Sensors 13, 15708–15725.

Zhang, L., Yao, Y., Peng, W., Shan, L., He, Y., Kong, J., 2019a. Real-time global ionospheric map and its application in single-frequency positioning. Sensors 19, 1138.

Zhang, X., Andersen, O., 2006. Surface ice flow velocity and tide retrieval of the Amery ice shelf using precise point positioning. J. Geod. 80 (4), 171–176.

Zhang, Y., Kubo, N., Chen, J., Wang, J., Wang, H., 2019b. Initial positioning assessment of BDS new satellite and new signal. Remote Sens. 11 (11), 1320.

Zhang, Y., Chen, J., Gong, X., Chen, Q., 2020. The update of BDS-2 TGD and its impact on positioning. Adv. Space Res. 65 (11), 2645–2661.

Zhou, F., Dong, D., Li, P., Li, X., Schuh, H., 2019. Influence of stochastic modeling for inter-system biases on multi-GNSS undifferenced and uncombined precise point positioning. GPS Solut. 23, 59.

Zumberge, J., Heflin, M., Jefferson, D., Watkins, M., Webb, F.H., 1997. Precise point positioning for the efficient and robust analysis of GPS data from large networks. J. Geophys. Res. Solid Earth 102 (B3), 5005–5017.